JACS
JOURNAL OF THE AMERICAN CHEMICAL SOCIETY

pubs.acs.org/JACS

Article

Supramolecular Double Helices from Small C_3-Symmetrical Molecules Aggregated in Water

René P. M. Lafleur,[#] Svenja Herziger,[#] Sandra M. C. Schoenmakers, Arthur D. A. Keizer, Jahaziel Jahzerah, Bala N. S. Thota, Lu Su, Paul H. H. Bomans, Nico A. J. M. Sommerdijk, Anja R. A. Palmans, Rainer Haag, Heiner Friedrich, Christoph Böttcher,* and E. W. Meijer*

Cite This: J. Am. Chem. Soc. 2020, 142, 17644−17652

Read Online

ACCESS | Metrics & More | Article Recommendations | Supporting Information

ABSTRACT: Supramolecular fibers in water, micrometers long and several nanometers in width, are among the most studied nanostructures for biomedical applications. These supramolecular polymers are formed through a spontaneous self-assembly process of small amphiphilic molecules by specific secondary interactions. Although many compounds do not possess a stereocenter, recent studies suggest the (co)existence of helical structures, albeit in racemic form. Here, we disclose a series of supramolecular (co)polymers based on water-soluble benzene-1,3,5-tricarboxamides (BTAs) that form double helices, fibers that were long thought to be chains of single molecules stacked in one dimension (1D). Detailed cryogenic transmission electron microscopy (cryo-TEM) studies and subsequent three-dimensional-volume reconstructions unveiled helical repeats, ranging from 15 to 30 nm. Most remarkable, the pitch can be tuned through the composition of the copolymers, where two different monomers with the same core but different peripheries are mixed in various ratios. Like in lipid bilayers, the hydrophobic shielding in the aggregates of these disc-shaped molecules is proposed to be best obtained by dimer formation, promoting supramolecular double helices. It is anticipated that many of the supramolecular polymers in water will have a thermodynamic stable structure, such as a double helix, although small structural changes can yield single stacks as well. Hence, it is essential to perform detailed analyses prior to sketching a molecular picture of these 1D fibers.

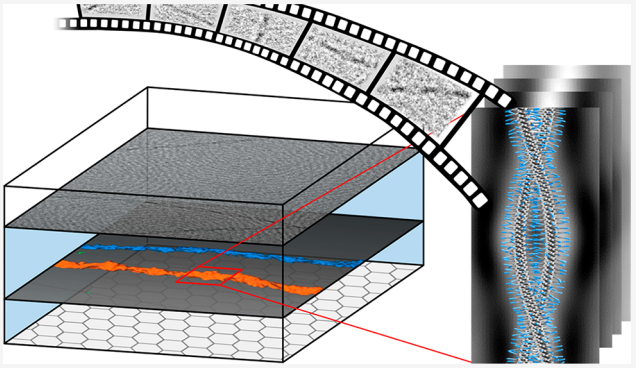

INTRODUCTION

The structure and function of biological macromolecules and synthetic polymers are intimately connected. Structural studies are therefore key to our understanding of how these macromolecules operate in their (biological) environment. Whereas groundbreaking structural studies on, for example, G-protein coupled receptors, ribosomes, and ion channels were performed using X-ray crystallography,[1−3] recent technical developments in cryogenic transmission electron microscopy (cryo-TEM) are currently accelerating their structural characterization.[4−13] Single-particle cryo-TEM allows researchers to obtain high-resolution structures through the imaging of many identical copies of biological assemblies.[14] In the past few years, one-dimensional (1D) supramolecular polymers that are formed from proteins involved in neurodegenerative diseases were characterized in great detail as well.[15−17] In patient-derived material, the polymers were observed to display different 3D architectures depending on the disease, illustrating the importance of detailed analyses.[16,17]

For synthetic 1D supramolecular polymers, such structure-to-function relationships also exist. For example, the self-assembled architectures formed from building blocks as simple as tripeptides can be used to control the optical and electrochemical properties of pigments.[18] In addition, the morphology of supramolecular nanostructures formed from tetrapeptides has been shown to affect their therapeutic potential.[19] Photocatalytic hydrogen production was observed with supramolecular polymers that feature a crystalline packing of chromophores.[20] Because of the high order in the packing of the molecules, such polymers can be structurally characterized in great detail.[20,21] However, usually, synthetic supramolecular polymers lack any form of high order or periodicity at the nanometer level.[22] Drawing molecular models that fit the nanoscopic to microscopic dimensions of the synthetic polymers is therefore common practice. To experimentally determine the molecular packing of noncrystalline architectures, one cannot rely on many atomically identical copies, as

Received: July 29, 2020
Published: September 16, 2020

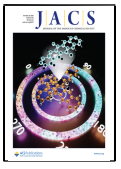

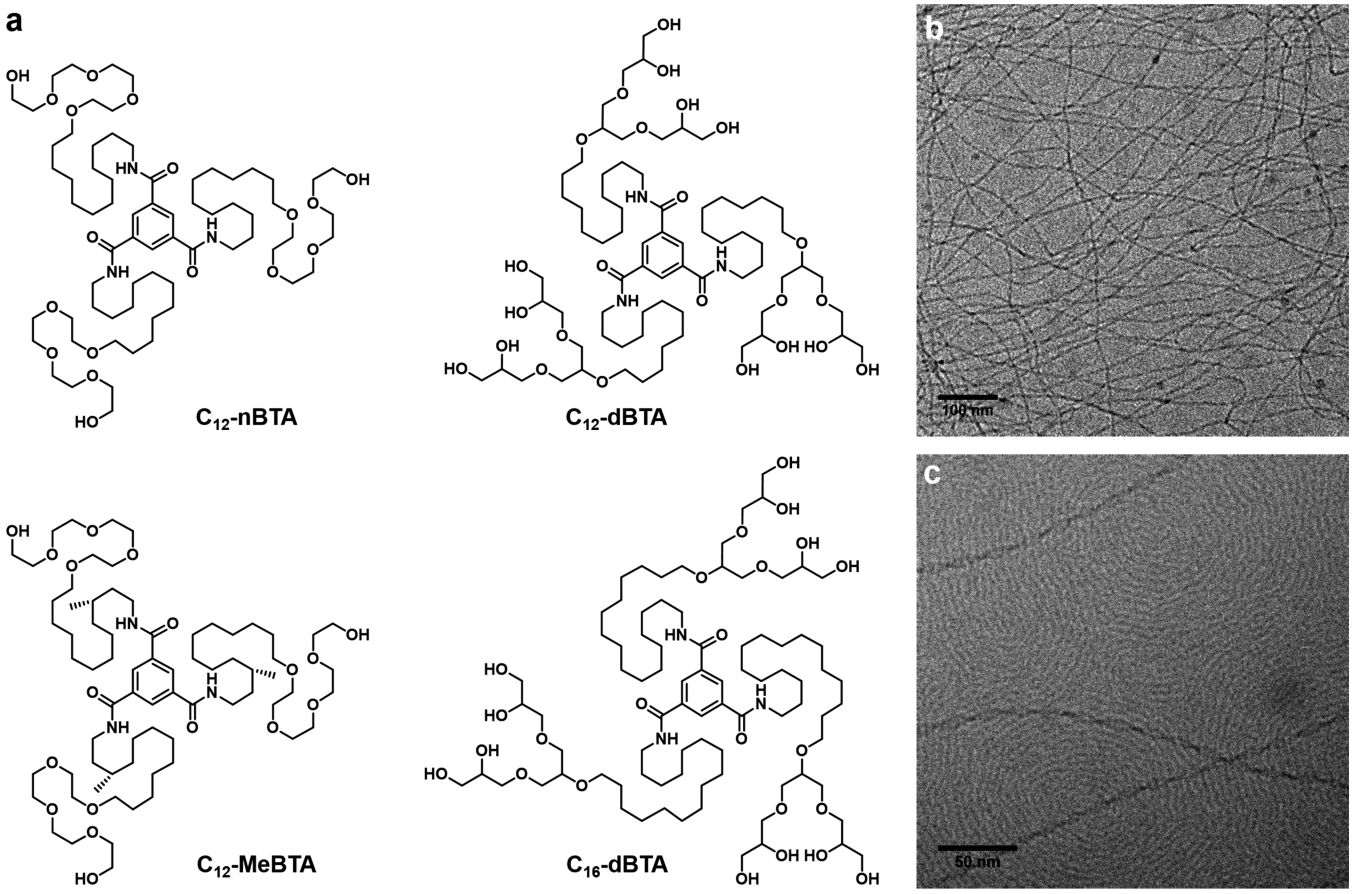

Figure 1. Molecular structures and cryo-TEM images of C_{12}-nBTA. (a) Chemical structures of **C_{12}-nBTA**, **C_{12}-dBTA**, **C_{12}-MeBTA**, and **C_{16}-dBTA**. Cryo-TEM images of supramolecular polymers formed from **C_{12}-nBTA** at a concentration of 0.75 mg/mL in H_2O (b) at a point resolution of 5 nm, as obtained from the contrast transfer function (CTF) at a defocus value of −10 μm (scale bar = 100 nm), and (c) at a point resolution of 2.4 nm as obtained from the CTF at a defocus value of −3 μm (scale bar = 50 nm).

compared to the biological macromolecules. Moreover, recent studies show that these one-dimensional assemblies often exhibit a diversity in molecular order and hence molecular dynamics.[23] For these reasons, the number of synthetic supramolecular polymers resolved at molecular resolution pales in comparison to the biological macromolecules and is a major hurdle to overcome in this part of nanotechnology.[24]

Cryo-TEM is also of crucial importance for the direct structural characterization of solution-born nanostructures.[24−29] When multiple views from different directions of a self-assembled aggregate are combined, cryo-electron tomography (cryo-ET) can yield three-dimensional (3D) information that cannot be obtained using any other experimental technique.[30,31] Recent developments allow researchers to better visualize organic structures in their native solution environment, including the introduction of graphene oxide (GOx) supports to realize thin but mechanically stable samples.[32] In addition, the use of a Volta phase plate during image acquisition allows one to enhance the contrast without sacrificing resolution.[4,33] Attractive candidates for these three-dimensional structural characterizations are synthetic supramolecular polymers in water, structures that are key components for the development of biomaterials in nanomedicine.[34] We selected polymers that are formed from amphiphiles with a benzene-1,3,5-tricarboxamide core (BTAs, Figure 1a).[35] Super-resolution microscopy showed micrometer-long fibers, but the resolution was not high enough to determine the exact diameter of several nanometers.[36] Cryo-TEM imaging showed fibers with some periodicity; however, it was impossible to decide on the structure at the molecular level.[35] Hence, most publications where these polymers were studied used cartoons of stacks of single molecules. These polymers were recently observed to be less dynamic than expected.[37] The full deuteration of polymers that were diluted from H_2O into excess D_2O for hydrogen/deuterium exchange experiments required multiple days,[37] and the polymers are remarkably resistive to disassembly by a good solvent.[38] When mixed with more water-soluble analogues, the obtained copolymers became even more stable in time.[39] Similar results have been recently obtained with BTAs that have carbohydrate groups at the periphery.[40] In the past, we were never able to elucidate the detailed structure of such fibers. For that, advanced cryo-TEM and analyses are required to characterize these polymers at a length scale that is close to the resolution and noise limit.

Here, we show that these BTA molecules can assemble into different architectures in water. To our surprise, most of the species present are double helices, and the pitch can be tuned by the composition of the fibers. Two of the BTA-based monomers contain three linear C_{12}-aliphatic tails that are covalently attached to a linear tetra(ethylene glycol) or a dendritic oligoglycerol-based side chain, **C_{12}-nBTA** and **C_{12}-dBTA**, respectively. One BTA molecule, **C_{12}-MeBTA**, is similar to **C_{12}-nBTA** but with a stereogenic center in the

https://dx.doi.org/10.1021/jacs.0c08179
J. Am. Chem. Soc. 2020, 142, 17644−17652

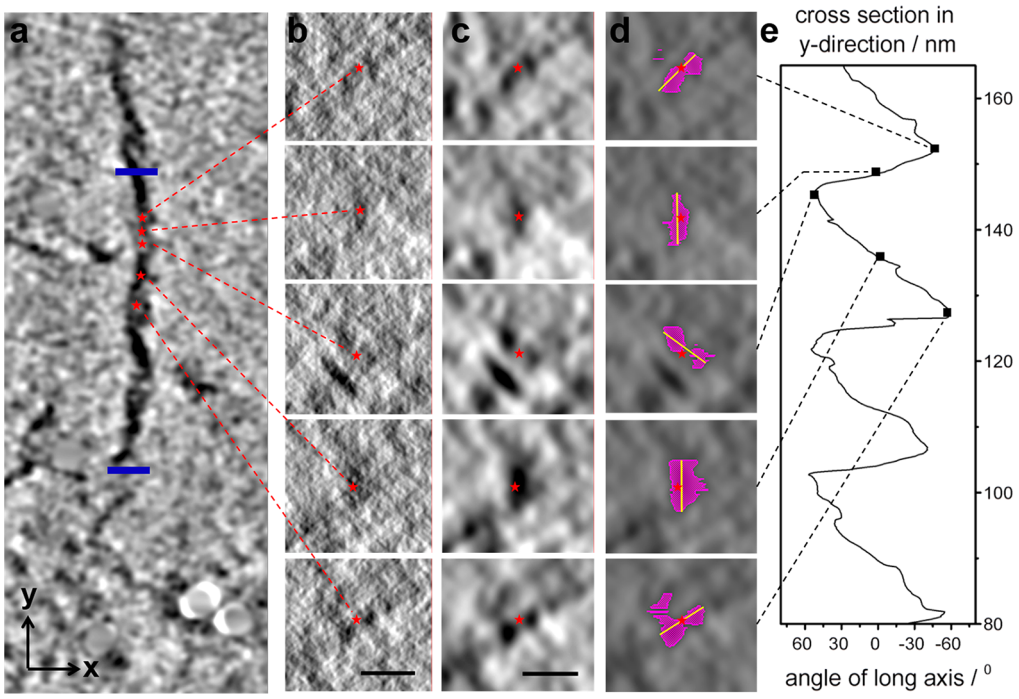

Figure 2. Analysis of the **C_{12}-nBTA** polymer in 3D. (a) Numerical cross section parallel to the **C_{12}-nBTA** polymer from the NAD-filtered tomographic reconstruction (average over 15 slices, 2.8 nm). The red stars indicate the positions at which vertical numerical cross sections (x−z planes) were extracted, which lay perpendicular to the long axis of the polymer. Their (x,y,z)-coordinate is the same in the rows of columns b, c, and d. The part of the polymer between the blue bars was analyzed in detail to construct the graph shown in panel e. (b) Vertical numerical cross sections (average over 10 slices, 1.9 nm) of the median-filtered data and (c) the NAD-filtered data. The high contrast ellipse below the red star in the middle image originates from another supramolecular polymer that is in proximity, and oriented with its long axis in the x-direction. (d) Vertical cross sections of the NAD-filtered data with, in magenta, an overlay of the segmented area(s), and, in yellow, the long axis of the ellipses that were fitted to the largest segmented areas. Some oversegmentation can be observed in the bottom image. (e) The angle at which the long axis of the fitted ellipse is observed (horizontal axis) is plotted as a function of the position along the polymer (vertical axis). The black squares in this graph correspond to the angles of the long axis that are displayed in yellow in d, which are −45°, 1°, 54°, 0°, and −58° from top to bottom. The scale bars are 10 nm and the magnifications are the same in columns b and c.

C_{12}-aliphatic tail. In another structure, **C_{16}-dBTA**, the dendritic oligoglycerol-based BTA has a C_{16}-aliphatic tail (Figure 1a). The ethylene glycol and glycerol units enable water solubility of the supramolecular polymers, whereas the aliphatic tails are required to shield the hydrogen bonds between the amides when the monomers stack on top of one another from water.[41] Given the influence of temperatures encountered during the assembly process,[42] the supramolecular polymers and copolymers were all prepared using the same heating−cooling protocol.[37] First, a detailed analysis of the polymers formed from the **C_{12}-nBTA** will be given, followed by the other three molecules in Figure 1a. Finally, we present the structures of the copolymers that are formed by mixing **C_{12}-nBTA** with both **C_{12}-dBTA** and **C_{16}-dBTA**.

RESULTS AND DISCUSSION

Double Helix of C_{12}-nBTA by Electron Microscopy. Conventional cryo-TEM imaging (0° projections) results in enough contrast to observe the high-aspect ratio supramolecular polymers formed by **C_{12}-nBTA** (Figure 1b). The very long 1D polymers have a diameter below 10 nm and polymer ends cannot be observed. Interestingly, when we were fortunate to have a thin vitrified film and used zero loss energy filtering, the contrast is enhanced such that also a fingerprint-like pattern becomes visible. The image in Figure 1c has been recorded at a nominal magnification of 61000× and is dominated by a fingerprint-like pattern that consists of uniformly spaced dark lines. Fast Fourier transforming of the images shows that the observed spacing is about 4.7 nm (Figure S1). The width of the hydrophobic part of **C_{12}-nBTA** is between 2 and 2.5 nm, which is roughly half the width of the repeat pattern of the fingerprint. Hence, we conclude that the dark lines originate from the more densely packed part of the **C_{12}-nBTA**, which is the benzene core and the aliphatic tails. The bright interspaces are assigned to hydrated ethylene glycol, known to have an electron density comparable to vitrified water and hence to create poor contrast. It is hypothesized that the fingerprint originates from **C_{12}-nBTA** molecules that are assembled at the air−water interface into long polymers (*vide infra*).[43]

Next to the fingerprint pattern, fibers can be clearly observed. When the long axis of the polymers is followed, there is a clear undulating variation in the diameter of the polymers (Figure 1c, Figure S2). 3D data is required to study the structure of the polymers in detail. However, the difference in contrast between the polymers and the surrounding vitrified water is small. To improve the signal-to-noise ratio in the images, we performed cryo-ET with vitrified films using GOx as a support layer to prepare thinner films (see Supporting Information),[32] combined with zero-loss energy filtering. The sample was tilted from −64° to +64°, and low-dose electron diffraction spots at 2 Å, recorded after the tomographic tilt series, confirm the presence of a GOx support layer (Figure S3). Alignment and reconstruction of the tilt series was

https://dx.doi.org/10.1021/jacs.0c08179
J. Am. Chem. Soc. 2020, 142, 17644−17652

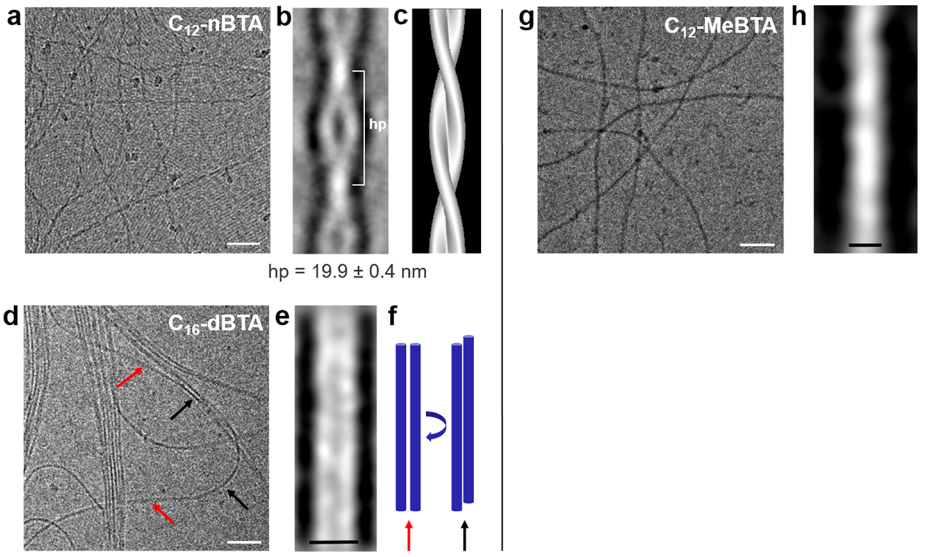

Figure 3. Structural analysis of the polymers formed by **C_{12}-nBTA**, **C_{16}-dBTA**, and **C_{12}-MeBTA**. (a) Cryo-TEM image of **C_{12}-nBTA** polymers that was used for image analysis. (b) Class sum image of the 100 best aligned individual extracts, revealing the pattern of a double helix with a defined half pitch of hp = 19.9 (±0.4) nm. (c) Surface representation of the volume reconstruction from the sum image (b) according to a previously reported helix reconstruction scheme.[52] (d) Cryo-TEM image of **C_{16}-dBTA** polymers. (e) Class sum image of aligned image extracts with a diameter of 6.3 (±0.4) nm for the pair of two stacks, with a random pitch. (f) Schematic showing the orientation of the two stacks relative to each other upon twisting. Arrows correspond to the two different orientations as indicated in (d). The diameter is approximately halved 2.9 (±0.4) nm at a side view orientation. (g) CryoTEM image of **C_{12}-MeBTA** polymers. (h) Class sum image of aligned image extracts reveals a motif consisting of a single stack with a diameter of 3.7 (±0.4) nm. Scale bars are 50 nm (a,d,g), 6 nm (e), and 3.5 nm (h).

subsequently performed in the software IMOD using the simultaneous iterative reconstruction technique.[44,45] While varying the *z*-height of numerical cross sections through the reconstructed volume, we observed parts of the regular fingerprint pattern described above. This structure can be visualized entirely when tilting the cross section to become parallel to the air−water interface, indicating that the structure is present only on the air−water interface of the vitrified film (Figure S4 and Movie S1). Hence, this result confirms our hypothesis that the **C_{12}-nBTA** polymers form a self-assembled monolayer (SAM) at the air−water interface, which consists of orderly positioned molecules. Because of the small width of the hydrophobic part of **C_{12}-nBTA** (∼2−2.5 nm) that gives the contrast, and the fact that the fingerprint pattern can be observed only within a few nanometers in *z*-height at the interface, it is most likely that the molecules are organized in an edge-on orientation at the air−water interface (Figure S5). In addition to the SAM, we have observed small aggregates that are less than 3 nm wide (Figure S6).

To enhance the visibility of the **C_{12}-nBTA** supramolecular polymers, the signal-to-noise ratio of the reconstructed volume was improved by denoising using either a 3D median filter or a nonlinear anisotropic diffusion (NAD) filter.[46] Subsequently, a numerical cross section was obtained in which the polymers are visible but not the SAM to allow an unbiased analysis of the polymers. Again, variations in the diameter of the polymers can be observed (Figure S7). The sizes of the smallest and largest diameters in the not-denoised volume are the same as those detected in Figure 1c (Figures S2 and S8). Remarkably, also the contrast along the length of the polymers appears to be not constant when all contrast from the polymer is included in the intensity averaged cross section (white box in Figure S7). We have reported similar observations also in the first paper on this molecule, but based on conventional cryo-TEM imaging.[35] The 3D structures that could give rise to these variations in the contrast and the diameter of the polymers are a double helix and a twisted ribbon.[47] Now, the improved contrast by using GOx and zero-loss energy filtering, and cryo-ET, allow for an in-depth analysis of the polymers in 3D.

To further investigate the polymers, we segmented two of them manually, which yielded 3D models of the polymers (see Supporting Information). Using a computer-aided visualization through the long axis of these polymers, we observe that the cross sections perpendicular to the long axis of the polymers are twisting in one direction (Movie S2). One of the polymers was carefully analyzed using its 3D model as a guide. At several locations along the polymer, which are indicated by the red stars in Figure 2a, we extracted vertical numerical cross sections (*x*−*z* planes) (Figure 2b). These provide a clearer view after denoising with NAD, and two separate dark spots are observed on opposite sides of the red stars in the top, middle, and bottom images (Figure 2c). In the other two images, which correspond to the high-contrast locations in Figure 2a, these separate dark spots merge into dark ellipses because of missing wedge artifacts.[48] Since the high-contrast areas are not connected in the parts of the polymer in which this artifact does not play a role, there must be two separate stacks oriented side by side. Hence, this observation excludes the interpretation of a twisted ribbon structure. Instead, and intriguingly, this analysis on a length scale of several nanometers indicates that two separate stacks of the achiral **C_{12}-nBTA** exist, and that these wrap around one another to form a double helix. The width of the dark spots (∼2 nm, Figure S9) matches the estimated diameter of the hydrophobic part of the molecule. In addition, the diameter of the polymers as observed in both 2D and 3D (∼6 nm, Figures S2, S8, and S9) corresponds to the 6 nm diameter that was previously found through small-angle X-ray scattering.[49]

Subsequently, we investigated the periodicity in the twisting nature of the double helix. We fitted the segmented areas in the

https://dx.doi.org/10.1021/jacs.0c08179
J. Am. Chem. Soc. 2020, 142, 17644−17652

$x-z$ planes with an ellipse and calculated the angles of the long axis (yellow lines in Figure 2d) of these ellipses. These yellow lines indicate the directions in which the two stacks lie side by side, resulting in the graph as displayed in Figure 2e. The angles gradually increase from about −60° to +60° and subsequently drop more quickly to −60°, and this pattern has a constant period. Such a sawtooth pattern is expected for a continuous twist in one direction, and angles with absolute values between 60° and 90° are not observed because of missing wedge artifacts. The analysis of the periodicity in 3D has been performed for both segmented polymers, and the combined data yield an average period of 23 (±2) nm (Figure S10). Gratifyingly, this period is in excellent agreement with measurements performed on a high-resolution conventional cryo-TEM image: 23 (±1) nm (Figure S11).

After this analysis in 3D with an unexpected outcome, we pursued an interpretation of the **C_{12}-nBTA** polymers beyond any doubt. We switched to a different electron microscope that is equipped with a Volta phase plate and a direct electron detector and recorded additional 2D images. Subsequently, we applied a completely different helical reconstruction approach to study the structure of the polymers. To this end, 380 environments containing the double helix repeat were extracted from different polymers and images, band-pass-filtered to remove both low- and high-frequency noise, and then translationally and rotationally aligned to create a sum image with improved signal-to-noise ratio. Because of the random orientation of the fingerprint, it disappears upon summing of the excerpts. In addition, multivariate statistical analysis (MSA) was applied to identify and remove those polymers for which the alignment is not possible because of the prevailing impact of the fingerprint or other distortions such as bending or tilting of the fibers.[50] For processing, the contrast was inverted, resulting in bright structures on a dark background. The resulting sum image of perfectly aligned and straight fiber segments (Figure 3b) shows a very accurate density separation of the double helix repeat (white) from the surrounding area (black seam). It exhibits a vertical mirror axis through the center of the image that is characteristic of a double helix. This structure is reminiscent of the internal packing of protofilaments in amyloid fibrils that are composed of paired β-sheets.[51] The class sum images of such protofilaments also show two high-density areas separated by an area of lower density, with a similar axial symmetry along the long axis of the filaments. The individual stacks of the polymers have a diameter of ∼3.5 nm, which is only slightly larger than that in the fingerprint at the air−water interface. The area between the stacks is gray and not black, implying that the individual stacks of BTAs are not completely apart from one another all the time. Transient local interactions between the two stacks of **C_{12}-nBTA** polymers are expected to occur that may stabilize the double helix. The helical symmetry of the structure allows us to calculate the 3D volume from the sum image.[52] The surrounding areas of the double helix repeat in **C_{12}-nBTA** were masked, and the part of the sum image corresponding to the helix pitch (in agreement with the tomography data) was cyclically shifted in a vertical direction in 360 steps. These are the equivalent of 1° rotation steps of the double helix around the long axis and enable a complete 3D reconstruction of the volume. The resulting 3D reconstruction of one full pitch of the double helix (Figure 3c) and its length corroborate our previous observations (*vide supra*). It must be noted that the assembled molecules are achiral and no preferred handedness is expected. Therefore, we refrain from discussing the handedness of the double helices, which in principle is present in equal amounts of P and M helices.

Influence of Molecular Changes on the Fiber Structure. Next, we investigated several different supramolecular polymers formed by the other molecules—all based on the BTA core—as displayed in Figure 1a. The water solubility of the **C_{12}-nBTA** was increased by substituting the tetra(ethylene glycol) unit with a dendritic oligoglycerol-based side chain at the C_{12}-aliphatic tail. As a result, the **C_{12}-dBTA** aggregates only into spherical micelles (Figure S13).[39] Therefore, we re-established the balance between the hydrophobic and hydrophilic parts by increasing the aliphatic tail with 4 methylene units in **C_{16}-dBTA** (see Supporting Information). Gratifyingly, cryo-TEM images of **C_{16}-dBTA** show that this molecule indeed forms supramolecular polymers (Figure 3d). After the techniques discussed above were applied, the results show that now two stacks are connected, not in a double helix, but as two adjacent stacks that appear as pairs (Figure 3e), as schematically shown in Figure 3f. Upon rotation along the structure, the overall width of the polymer changes by half (Figure 3d,f). This is confirmed by MSA and subsequent classification of a randomly extracted set of fiber environments. In the cryo-TEM images these pairs of two stacks are observed to bundle with other pairs, but also observed as individual pairs. However, no single stacks are observed because of the changes in the width of the polymers following their long axis. These ribbon-like structures differ significantly in their appearance as compared to the double helices because their contrast and thickness varies while they rotate in the volume. By rotation of a pair of two stacks like the one in Figure 3e by 90°, a motif with the diameter of a single stack 2.9 (±0.4) nm is obtained (not shown).

To show how subtle differences in the molecular structure influence the morphology, we show the cryo-TEM analysis of **C_{12}-MeBTA** (Figure 3g,h). The **C_{12}-MeBTA** is a chiral analogue with three methyl groups more than **C_{12}-nBTA** that also forms supramolecular polymers.[35] Previous work showed that **C_{12}-MeBTA** polymers have more order in the arrangement of the BTA cores because of more persistent hydrogen bonds.[49] After cryo-TEM imaging and generating a class sum image, the fibers look like a single unstructured polymer stack with a diameter of 3.7 (±0.4) nm (Figure 3h). The distinguished organization into two individual stacks as observed with **C_{12}-nBTA** and **C_{16}-dBTA** is obviously lost here. Moreover, MSA and subsequent classification revealed the tendency of the fibers to twist (Figure S14). These results show that careful analyses are a prerequisite for discriminating the differences in the 1D packing of supramolecular polymers that are caused by small differences in the molecular structure of the monomers. In the next section we continue by studying supramolecular copolymers.

Electron Microscopy of Mixtures of C_{12}-dBTA and C_{16}-dBTA with C_{12}-nBTA. We studied mixtures of both dendritic BTAs (**C_{12}-dBTA** and **C_{16}-dBTA**) with **C_{12}-nBTA** in different ratios. For the combination of **C_{12}-nBTA** and **C_{12}-dBTA** we have shown before that they copolymerize in ratios of 2:1, 1:1, and 1:2.[39] After both molecules were mixed, the same heating−cooling protocol was used to be consistent with the sample preparation of the homopolymers (see Supporting Information). During this protocol the molecules are heated to 80 °C, which is above their cloud point temperature,[53] and this is likely causing a temporal dehydration of the ethylene glycol

https://dx.doi.org/10.1021/jacs.0c08179
J. Am. Chem. Soc. 2020, 142, 17644−17652

and glycerol units. Similar to above, cryo-TEM micrographs of the respective copolymer samples were recorded and these were subsequently analyzed by MSA and classification techniques.

For the three C_{12}-nBTA/C_{12}-dBTA mixtures, several micrometers-long supramolecular polymers are observed as the dominant morphology (Figure S15). In Figure 4a

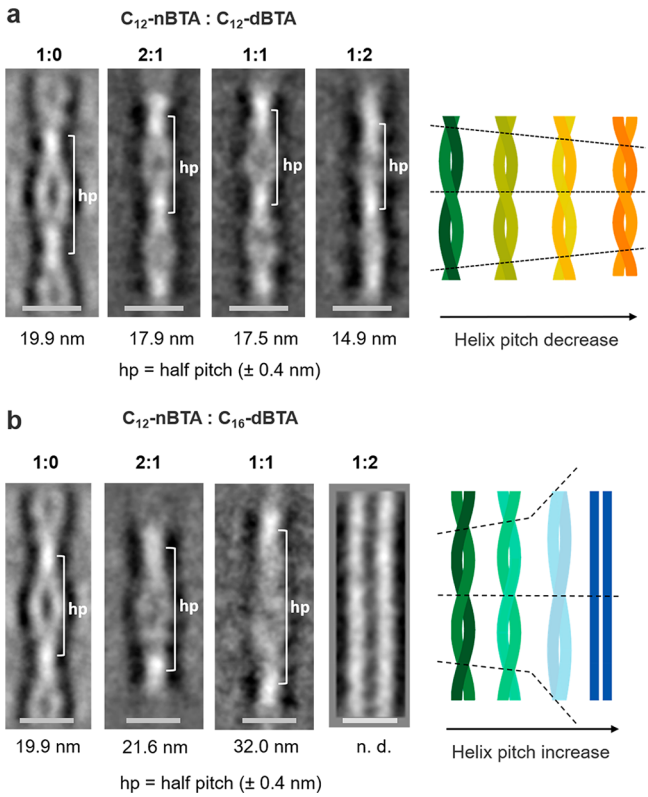

Figure 4. Structural analysis of supramolecular copolymers. (a) Class sum images for different molar ratios of C_{12}-nBTA and C_{12}-dBTA. The amount of C_{12}-dBTA increases from left to right, and the corresponding lengths of the half pitch are indicated. (b) Class sum images for different molar ratios of C_{12}-nBTA and C_{16}-dBTA. The amount of C_{16}-dBTA increases from left to right, and the corresponding lengths of the half pitch are indicated. The cartoons on the right-hand side of the figure show the changes in the pitch of the double helix and follow the same sequence as the class sum images, and different colors are used for the different copolymers. The scale bar is 10 nm in all cases.

representative class sum images of the copolymers are shown next to the sum image of C_{12}-nBTA. The structures of the 2:1 and 1:1 copolymers are also double helices. Both class sum images are representative, which means that most images show a double helix with only slight variations. The length of the half pitch of the double helices is determined to be 17.9 (±0.4) nm and 17.5 (±0.4) nm for the 2:1 and 1:1 copolymers, respectively. These values are significantly shorter than the 19.9 (±0.4) nm of the pure C_{12}-nBTA. The 1:2 copolymers look slightly different because the double helix seems to vanish (Figure 4a). However, an undulation in the density along the polymer can still be observed, with a half pitch of 14.9 (±0.4) nm, which is even shorter as compared to those of the 2:1 and 1:1 copolymers. Although no distinct separation between two individual stacks can be deduced for the 1:2 copolymer, the similar alternating pattern indicates that either a twisted stack is formed or that more than one stack of molecules interact with one another, as observed for the other compositions. These delicate variations in the length of the half pitch, depending on the composition, indicate that the polymers are likely well mixed at the molecular level and thus probably form copolymers with a regular composition.

The C_{12}-nBTA assembles into a double helix and the C_{16}-dBTA assembles into a pair consisting of two adjacent stacks (*vide supra*). Micrometers-long supramolecular polymers were also found as the dominant morphology for all mixtures of C_{12}-nBTA and C_{16}-dBTA. Despite the similarities in the cryo-TEM data at first view (Figure S16), also here subtle differences are observed in the images. In the case of the 2:1 and 1:1 copolymer, both twisted and ribbon-like morphologies are observed upon detailed analysis. For the 1:2 copolymer, individual fibers are observed predominantly, although bundles of these fibers are also observed. The variety of aggregates shows the flexibility and adaptivity of supramolecular copolymers. Subtle variations in the parameters of the preparation process can influence the resulting morphologies and induce multiple aggregation types, even within one sample. After qualitatively evaluating similarities and differences in the images, we focus on individual and structurally defined polymers for which structural analysis by MSA and subsequent classification of the cryo-TEM data appeared possible. The resulting class sum images for all copolymers of C_{12}-nBTA and C_{16}-dBTA are shown in Figure 4b. For the 2:1 mixture a double helix can be observed with a half pitch of 21.6 (±0.4) nm, slightly larger as compared to those of the C_{12}-nBTA homopolymers. When the amount of C_{16}-dBTA is increased, resulting in a ratio of 1:1, also a double helix is detected and for this copolymer a half pitch of 32.0 (±0.4) nm is determined. For the 1:2 mixture we observe a different structure, which is comparable to the homopolymers formed by C_{16}-dBTA itself and has two parallel stacks with diameters of 2.2 (±0.4) nm each. The overall width of the structure is determined to be 6.7 (±0.4) nm. According to the measured diameters, these polymers are likely composed of two stacks that each consist of a one-dimensional pile of the molecules. The two parallel stacks can therefore be thought of as a double helix with an infinitely long pitch. Thus, the copolymerization of C_{12}-nBTA with an increasing amount of C_{16}-dBTA leads to the unwinding of the supramolecular double helix. Similar to those of the mixtures with C_{12}-dBTA, the gradual change in the length of the half pitch suggests the formation of random copolymers.

CONCLUSIONS

By using detailed cryo-TEM and cryo-ET analyses with a wide variety of approaches, we have shown that supramolecular polymers in water—counterintuitively and against the current understanding—can form double helices. For the different BTA-based supramolecular polymers, we often observe structural diversity, but herein the presence of significant amounts of double helices that are micrometers long is reported. These double helices are observed in combination with single-stacked polymer monolayers at the air−water interface and smaller highly dynamic aggregates that are difficult to characterize. Most remarkable, in most cases the stable structure is a double helix with a regular repeat of which the length (specified as half pitch) varies with the molecular structure of the monomer as well as the composition of monomers in the supramolecular copolymers. In some cases,

https://dx.doi.org/10.1021/jacs.0c08179
J. Am. Chem. Soc. 2020, 142, 17644−17652

even an infinite pitch is observed when two adjacent stacks that do not twist are present. The double helix structure was discovered for the **C_{12}-nBTA** through direct observation in 3D using cryo-ET. The regular period of ~23 nm is remarkable given that the structure originates from an achiral molecule. This allowed us to analyze the polymers with a complementary approach that uses components of the single particle analysis method (alignment, multivariate statistical analysis, and classification), and subsequently perform an image-based 3D helical reconstruction. Another remarkable observation is the lack of helical inversion observed in the double helices over long lengths. Obviously, the number of fibers analyzed is too small to prove the 50:50 ratio between left-handed and right-handed helices. In the vitrified films we did not observe double helices of which the two stacks separate or supramolecular polymers that consist of a stack of single molecules, except the ones at the air−water interface.

Upon mixing of BTA-based amphiphiles in different ratios, the length of the half pitch of the double helix changes in the copolymers. When **C_{12}-nBTA**, a double helix forming monomer, is mixed with **C_{16}-dBTA**, a monomer that forms a pair of two stacks, the double helix gets unraveled. In other words, when **C_{16}-dBTA** is the majority in the mixture, the helix adopts the straight pairing of the majority component. Upon mixing of **C_{12}-nBTA** with **C_{12}-dBTA**, a spherical micelle forming monomer, the double helix gets more twisted, resulting in a shorter pitch when more **C_{12}-dBTA** is added. These data are in-line with a very good mixing of the two molecules and suggests that the number of molecules of each type is more or less constant over each length of the half pitch, although hard evidence for that is lacking. To show that the double helix is not present in all cases, we also show the single-polymer stacks formed by **C_{12}-MeBTA**, which illustrates how subtle the assembly process is. Although great care was taken in always using the same assembly conditions, small variations in the preparation method of supramolecular polymers can also result in different morphologies. The results presented show the importance of an in-depth analysis of all structures formed and that, together with data on the dynamic exchange and insights into the mechanism of formation, it is possible to get a better understanding of the properties of these supramolecular assemblies.

Currently, it is experimentally impossible to elucidate which molecular interactions are responsible for the formation of the very regular double helix. Like in lipid bilayers, the hydrophobic shielding in the aggregates is proposed to be the best way to explain the dimer formation promoting double helices. However, this will require further advances in both microscopy and computational approaches. Some indications were already proposed in 2007 by Fejer and Wales. They explored the potential energy landscape for clustering disklike ellipsoidal particles and showed that fibers of one or more stacks can be obtained depending on the potential energy surface.[54] The double helix revealed in this study may be kinetically very stable and could therefore explain the slow monomer exchange of these polymers that was recently observed to occur during multiple days.[37] However, at present, it is still too difficult to directly correlate the dynamics of supramolecular polymers and their high-resolution structures. We anticipate that the accurate determination of 3D structures in water will be important to establish the structure−function relationships of man-made materials. Moreover, it is expected that many more 1D fibers presently thought to be single stacks turn out to be double helices.

■ ASSOCIATED CONTENT

Supporting Information

The Supporting Information is available free of charge at https://pubs.acs.org/doi/10.1021/jacs.0c08179.

Details on sample preparation and chemical synthesis, all details on how the TEM measurements were made and analyzed, and additional images (PDF)

Movie 1 (MOV)

Movie 2 (MOV)

■ AUTHOR INFORMATION

Corresponding Authors

E. W. Meijer − *Institute for Complex Molecular Systems, Eindhoven University of Technology, Eindhoven 5600 MB, The Netherlands;* orcid.org/0000-0003-4126-7492; Email: e.w.meijer@tue.nl

Christoph Böttcher − *Research Center of Electron Microscopy and Core Facility BioSupraMol, Institute of Chemistry and Biochemistry, Freie Universität Berlin, Berlin 14195, Germany;* Email: christoph.boettcher@fzem.fu-berlin.de

Authors

René P. M. Lafleur − *Institute for Complex Molecular Systems, Eindhoven University of Technology, Eindhoven 5600 MB, The Netherlands;* orcid.org/0000-0003-0026-3428

Svenja Herziger − *Institute of Chemistry and Biochemistry and Research Center of Electron Microscopy and Core Facility BioSupraMol, Institute of Chemistry and Biochemistry, Freie Universität Berlin, Berlin 14195, Germany*

Sandra M. C. Schoenmakers − *Institute for Complex Molecular Systems, Eindhoven University of Technology, Eindhoven 5600 MB, The Netherlands*

Arthur D. A. Keizer − *Center of Multiscale Electron Microscopy, Department of Chemical Engineering and Chemistry, Eindhoven University of Technology, Eindhoven 5600 MB, The Netherlands*

Jahaziel Jahzerah − *Institute of Chemistry and Biochemistry, Freie Universität Berlin, Berlin 14195, Germany*

Bala N. S. Thota − *Institute for Complex Molecular Systems, Eindhoven University of Technology, Eindhoven 5600 MB, The Netherlands; Institute of Chemistry and Biochemistry, Freie Universität Berlin, Berlin 14195, Germany*

Lu Su − *Institute for Complex Molecular Systems, Eindhoven University of Technology, Eindhoven 5600 MB, The Netherlands;* orcid.org/0000-0001-8207-756X

Paul H. H. Bomans − *Institute for Complex Molecular Systems and Center of Multiscale Electron Microscopy, Department of Chemical Engineering and Chemistry, Eindhoven University of Technology, Eindhoven 5600 MB, The Netherlands*

Nico A. J. M. Sommerdijk − *Institute for Complex Molecular Systems and Center of Multiscale Electron Microscopy, Department of Chemical Engineering and Chemistry, Eindhoven University of Technology, Eindhoven 5600 MB, The Netherlands;* orcid.org/0000-0002-8956-195X

Anja R. A. Palmans − *Institute for Complex Molecular Systems, Eindhoven University of Technology, Eindhoven 5600 MB, The Netherlands;* orcid.org/0000-0002-7201-1548

Rainer Haag − *Institute of Chemistry and Biochemistry, Freie Universität Berlin, Berlin 14195, Germany*

https://dx.doi.org/10.1021/jacs.0c08179
J. Am. Chem. Soc. 2020, 142, 17644−17652

Heiner Friedrich − *Institute for Complex Molecular Systems and Center of Multiscale Electron Microscopy, Department of Chemical Engineering and Chemistry, Eindhoven University of Technology, Eindhoven 5600 MB, The Netherlands;* orcid.org/0000-0003-4582-0064

Complete contact information is available at: https://pubs.acs.org/10.1021/jacs.0c08179

Author Contributions

#R.P.M.L. and S.H. contributed equally to this work.

Notes

The authors declare no competing financial interest.

■ ACKNOWLEDGMENTS

We gratefully acknowledge A.J.H. Spiering for synthetic support. The authors acknowledge financial support from the Dutch Ministry of Education, Culture and Science (Gravity Program 024.001.035) and the ERC Advanced Grant SynMat (788618). H.G., S.H., and C.B. thank SFB765 of the German Science Foundation (DFG) for funding. E.W.M. thanks the Humboldt Foundation for support.

■ REFERENCES

(1) Rasmussen, S. G. F.; DeVree, B. T.; Zou, Y.; Kruse, A. C.; Chung, K. Y.; Kobilka, T. S.; Thian, F. S.; Chae, P. S.; Pardon, E.; Calinski, D.; Mathiesen, J. M.; Shah, S. T. A.; Lyons, J. A.; Caffrey, M.; Gellman, S. H.; Steyaert, J.; Skiniotis, G.; Weis, W. I.; Sunahara, R. K.; Kobilka, B. K. Crystal structure of the [bgr]2 adrenergic receptor-Gs protein complex. *Nature* **2011**, *477* (7366), 549−555.

(2) Ban, N.; Nissen, P.; Hansen, J.; Moore, P. B.; Steitz, T. A. The Complete Atomic Structure of the Large Ribosomal Subunit at 2.4 Å Resolution. *Science* **2000**, *289* (5481), 905−920.

(3) Doyle, D. A.; Morais Cabral, J.; Pfuetzner, R. A.; Kuo, A.; Gulbis, J. M.; Cohen, S. L.; Chait, B. T.; MacKinnon, R. The structure of the potassium channel: molecular basis of K+ conduction and selectivity. *Science* **1998**, *280* (5360), 69−77.

(4) Liang, Y.-L.; Khoshouei, M.; Radjainia, M.; Zhang, Y.; Glukhova, A.; Tarrasch, J.; Thal, D. M.; Furness, S. G. B.; Christopoulos, G.; Coudrat, T.; Danev, R.; Baumeister, W.; Miller, L. J.; Christopoulos, A.; Kobilka, B. K.; Wootten, D.; Skiniotis, G.; Sexton, P. M. Phase-plate cryo-EM structure of a class B GPCR−G-protein complex. *Nature* **2017**, *546* (7656), 118−123.

(5) Zhang, Y.; Sun, B.; Feng, D.; Hu, H.; Chu, M.; Qu, Q.; Tarrasch, J. T.; Li, S.; Sun Kobilka, T.; Kobilka, B. K.; Skiniotis, G. Cryo-EM structure of the activated GLP-1 receptor in complex with a G protein. *Nature* **2017**, *546* (7657), 248−253.

(6) Amunts, A.; Brown, A.; Bai, X.-c.; Llácer, J. L.; Hussain, T.; Emsley, P.; Long, F.; Murshudov, G.; Scheres, S. H. W.; Ramakrishnan, V. Structure of the Yeast Mitochondrial Large Ribosomal Subunit. *Science* **2014**, *343* (6178), 1485−1489.

(7) Desai, N.; Brown, A.; Amunts, A.; Ramakrishnan, V. The structure of the yeast mitochondrial ribosome. *Science* **2017**, *355* (6324), 528−531.

(8) Hite, R. K.; Tao, X.; MacKinnon, R. Structural basis for gating the high-conductance Ca2+-activated K+ channel. *Nature* **2017**, *541* (7635), 52−57.

(9) Park, E.; Campbell, E. B.; MacKinnon, R. Structure of a CLC chloride ion channel by cryo-electron microscopy. *Nature* **2017**, *541* (7638), 500−505.

(10) Tao, X.; Hite, R. K.; MacKinnon, R. Cryo-EM structure of the open high-conductance Ca2+-activated K+ channel. *Nature* **2017**, *541* (7635), 46−51.

(11) Loveland, A. B.; Demo, G.; Grigorieff, N.; Korostelev, A. A. Ensemble cryo-EM elucidates the mechanism of translation fidelity. *Nature* **2017**, *546*, 113.

(12) Butterwick, J. A.; del Mármol, J.; Kim, K. H.; Kahlson, M. A.; Rogow, J. A.; Walz, T.; Ruta, V. Cryo-EM structure of the insect olfactory receptor Orco. *Nature* **2018**, *560* (7719), 447−452.

(13) Pan, X.; Li, Z.; Zhou, Q.; Shen, H.; Wu, K.; Huang, X.; Chen, J.; Zhang, J.; Zhu, X.; Lei, J.; Xiong, W.; Gong, H.; Xiao, B.; Yan, N. Structure of the human voltage-gated sodium channel $Na_v1.4$ in complex with β1. *Science* **2018**, *362* (6412), eaau2486.

(14) Fernandez-Leiro, R.; Scheres, S. H. W. Unravelling biological macromolecules with cryo-electron microscopy. *Nature* **2016**, *537* (7620), 339−346.

(15) Li, B.; Ge, P.; Murray, K. A.; Sheth, P.; Zhang, M.; Nair, G.; Sawaya, M. R.; Shin, W. S.; Boyer, D. R.; Ye, S.; Eisenberg, D. S.; Zhou, Z. H.; Jiang, L. Cryo-EM of full-length α-synuclein reveals fibril polymorphs with a common structural kernel. *Nat. Commun.* **2018**, *9* (1), 3609.

(16) Fitzpatrick, A. W. P.; Falcon, B.; He, S.; Murzin, A. G.; Murshudov, G.; Garringer, H. J.; Crowther, R. A.; Ghetti, B.; Goedert, M.; Scheres, S. H. W. Cryo-EM structures of tau filaments from Alzheimer's disease. *Nature* **2017**, *547* (7662), 185−190.

(17) Falcon, B.; Zhang, W.; Murzin, A. G.; Murshudov, G.; Garringer, H. J.; Vidal, R.; Crowther, R. A.; Ghetti, B.; Scheres, S. H. W.; Goedert, M. Structures of filaments from Pick's disease reveal a novel tau protein fold. *Nature* **2018**, *561* (7721), 137−140.

(18) Lampel, A.; McPhee, S. A.; Park, H.-A.; Scott, G. G.; Humagain, S.; Hekstra, D. R.; Yoo, B.; Frederix, P. W. J. M.; Li, T.-D.; Abzalimov, R. R.; Greenbaum, S. G.; Tuttle, T.; Hu, C.; Bettinger, C. J.; Ulijn, R. V. Polymeric peptide pigments with sequence-encoded properties. *Science* **2017**, *356* (6342), 1064−1068.

(19) Wang, Y.; Kaur, K.; Scannelli, S. J.; Bitton, R.; Matson, J. B. Self-Assembled Nanostructures Regulate H_2S Release from Constitutionally Isomeric Peptides. *J. Am. Chem. Soc.* **2018**, *140* (44), 14945−14951.

(20) Weingarten, A. S.; Kazantsev, R. V.; Palmer, L. C.; McClendon, M.; Koltonow, A. R.; Samuel, A. P. S.; Kiebala, D. J.; Wasielewski, M. R.; Stupp, S. I. Self-assembling hydrogel scaffolds for photocatalytic hydrogen production. *Nat. Chem.* **2014**, *6* (11), 964−970.

(21) Shahar, C.; Baram, J.; Tidhar, Y.; Weissman, H.; Cohen, S. R.; Pinkas, I.; Rybtchinski, B. Self-Assembly of Light-Harvesting Crystalline Nanosheets in Aqueous Media. *ACS Nano* **2013**, *7* (4), 3547−3556.

(22) Krieg, E.; Bastings, M. M. C.; Besenius, P.; Rybtchinski, B. Supramolecular Polymers in Aqueous Media. *Chem. Rev.* **2016**, *116* (4), 2414−2477.

(23) Hendricks, M. P.; Sato, K.; Palmer, L. C.; Stupp, S. I. Supramolecular Assembly of Peptide Amphiphiles. *Acc. Chem. Res.* **2017**, *50* (10), 2440−2448.

(24) Berlepsch, H. v.; Ludwig, K.; Schade, B.; Haag, R.; Böttcher, C. Progress in the direct structural characterization of fibrous amphiphilic supramolecular assemblies in solution by transmission electron microscopic techniques. *Adv. Colloid Interface Sci.* **2014**, *208*, 279−292.

(25) Cui, H.; Hodgdon, T. K.; Kaler, E. W.; Abezgauz, L.; Danino, D.; Lubovsky, M.; Talmon, Y.; Pochan, D. J. Elucidating the assembled structure of amphiphiles in solution via cryogenic transmission electron microscopy. *Soft Matter* **2007**, *3* (8), 945−955.

(26) Zhong, S.; Pochan, D. J. Cryogenic Transmission Electron Microscopy for Direct Observation of Polymer and Small-Molecule Materials and Structures in Solution. *Polym. Rev.* **2010**, *50* (3), 287−320.

(27) Newcomb, C. J.; Moyer, T. J.; Lee, S. S.; Stupp, S. I. Advances in cryogenic transmission electron microscopy for the characterization of dynamic self-assembling nanostructures. *Curr. Opin. Colloid Interface Sci.* **2012**, *17* (6), 350−359.

(28) Friedrich, H.; Frederik, P. M.; de With, G.; Sommerdijk, N. A. J. M. Imaging of Self-Assembled Structures: Interpretation of TEM and Cryo-TEM Images. *Angew. Chem., Int. Ed.* **2010**, *49* (43), 7850−7858.

(29) Patterson, J. P.; Xu, Y.; Moradi, M.-A.; Sommerdijk, N. A. J. M.; Friedrich, H. CryoTEM as an Advanced Analytical Tool for Materials Chemists. *Acc. Chem. Res.* **2017**, *50* (7), 1495−1501.
(30) Evans, J. E.; Friedrich, H. Advanced tomography techniques for inorganic, organic, and biological materials. *MRS Bull.* **2016**, *41* (7), 516−521.
(31) McKenzie, B. E.; Friedrich, H.; Wirix, M. J. M.; de Visser, J. F.; Monaghan, O. R.; Bomans, P. H. H.; Nudelman, F.; Holder, S. J.; Sommerdijk, N. A. J. M. Controlling Internal Pore Sizes in Bicontinuous Polymeric Nanospheres. *Angew. Chem., Int. Ed.* **2015**, *54* (8), 2457−2461.
(32) van de Put, M. W. P.; Patterson, J. P.; Bomans, P. H. H.; Wilson, N. R.; Friedrich, H.; van Benthem, R. A. T. M.; de With, G.; O'Reilly, R. K.; Sommerdijk, N. A. J. M. Graphene oxide single sheets as substrates for high resolution cryoTEM. *Soft Matter* **2015**, *11* (7), 1265−1270.
(33) Danev, R.; Buijsse, B.; Khoshouei, M.; Plitzko, J. M.; Baumeister, W. Volta potential phase plate for in-focus phase contrast transmission electron microscopy. *Proc. Natl. Acad. Sci. U. S. A.* **2014**, *111* (44), 15635−15640.
(34) Webber, M. J.; Appel, E. A.; Meijer, E. W.; Langer, R. Supramolecular biomaterials. *Nat. Mater.* **2016**, *15* (1), 13−26.
(35) Leenders, C. M.; Albertazzi, L.; Mes, T.; Koenigs, M. M.; Palmans, A. R.; Meijer, E. W. Supramolecular polymerization in water harnessing both hydrophobic effects and hydrogen bond formation. *Chem. Commun.* **2013**, *49* (19), 1963−1965.
(36) Albertazzi, L.; van der Zwaag, D.; Leenders, C. M. A.; Fitzner, R.; van der Hofstad, R. W.; Meijer, E. W. Probing Exchange Pathways in One-Dimensional Aggregates with Super-Resolution Microscopy. *Science* **2014**, *344* (6183), 491−495.
(37) Lou, X.; Lafleur, R. P. M.; Leenders, C. M. A.; Schoenmakers, S. M. C.; Matsumoto, N. M.; Baker, M. B.; van Dongen, J. L. J.; Palmans, A. R. A.; Meijer, E. W. Dynamic diversity of synthetic supramolecular polymers in water as revealed by hydrogen/deuterium exchange. *Nat. Commun.* **2017**, *8*, 15420.
(38) Lafleur, R. P. M.; Lou, X.; Pavan, G. M.; Palmans, A. R. A.; Meijer, E. W. Consequences of a cosolvent on the structure and molecular dynamics of supramolecular polymers in water. *Chemical Science* **2018**, *9*, 6199−6209.
(39) Thota, B. N. S.; Lou, X.; Bochicchio, D.; Paffen, T. F. E.; Lafleur, R. P. M.; van Dongen, J. L. J.; Ehrmann, S.; Haag, R.; Pavan, G. M.; Palmans, A. R. A.; Meijer, E. W. Supramolecular Copolymerization as a Strategy to Control the Stability of Self-Assembled Nanofibers. *Angew. Chem., Int. Ed.* **2018**, *57* (23), 6843−6847.
(40) Hendrikse, S. I. S.; Su, L.; Hogervorst, T. P.; Lafleur, R. P. M.; Lou, X.; van der Marel, G. A.; Codee, J. D. C.; Meijer, E. W. Elucidating the Ordering in Self-Assembled Glycocalyx Mimicking Supramolecular Copolymers in Water. *J. Am. Chem. Soc.* **2019**, *141* (35), 13877−13886.
(41) Leenders, C. M. A.; Baker, M. B.; Pijpers, I. A. B.; Lafleur, R. P. M.; Albertazzi, L.; Palmans, A. R. A.; Meijer, E. W. Supramolecular polymerisation in water; elucidating the role of hydrophobic and hydrogen-bond interactions. *Soft Matter* **2016**, *12* (11), 2887−2893.
(42) Kemper, B.; Zengerling, L.; Spitzer, D.; Otter, R.; Bauer, T.; Besenius, P. Kinetically Controlled Stepwise Self-Assembly of AuI-Metallopeptides in Water. *J. Am. Chem. Soc.* **2018**, *140* (2), 534−537.
(43) Hamley, I. W. *Introduction to Soft Matter - Revised ed.: Synthetic and Biological Self-Assembling Materials*; John Wiley & Sons, Ltd.: 2007.
(44) Gilbert, P. Iterative methods for the three-dimensional reconstruction of an object from projections. *J. Theor. Biol.* **1972**, *36* (1), 105−117.
(45) Kremer, J. R.; Mastronarde, D. N.; McIntosh, J. R. Computer visualization of three-dimensional image data using IMOD. *J. Struct. Biol.* **1996**, *116* (1), 71−6.
(46) Frangakis, A. S.; Hegerl, R. Noise Reduction in Electron Tomographic Reconstructions Using Nonlinear Anisotropic Diffusion. *J. Struct. Biol.* **2001**, *135* (3), 239−250.
(47) Merg, A. D.; Boatz, J. C.; Mandal, A.; Zhao, G.; Mokashi-Punekar, S.; Liu, C.; Wang, X.; Zhang, P.; van der Wel, P. C. A.; Rosi, N. L. Peptide-Directed Assembly of Single-Helical Gold Nanoparticle Superstructures Exhibiting Intense Chiroptical Activity. *J. Am. Chem. Soc.* **2016**, *138* (41), 13655−13663.
(48) Orlova, E. V.; Saibil, H. R. Structural Analysis of Macromolecular Assemblies by Electron Microscopy. *Chem. Rev.* **2011**, *111* (12), 7710−7748.
(49) Baker, M. B.; Albertazzi, L.; Voets, I. K.; Leenders, C. M. A.; Palmans, A. R. A.; Pavan, G. M.; Meijer, E. W. Consequences of chirality on the dynamics of a water-soluble supramolecular polymer. *Nat. Commun.* **2015**, *6*, 6234.
(50) van Heel, M.; Frank, J. Use of multivariate statistics in analysing the images of biological macromolecules. *Ultramicroscopy* **1981**, *6* (2), 187−194.
(51) Fitzpatrick, A. W. P.; Debelouchina, G. T.; Bayro, M. J.; Clare, D. K.; Caporini, M. A.; Bajaj, V. S.; Jaroniec, C. P.; Wang, L.; Ladizhansky, V.; Müller, S. A.; MacPhee, C. E.; Waudby, C. A.; Mott, H. R.; De Simone, A.; Knowles, T. P. J.; Saibil, H. R.; Vendruscolo, M.; Orlova, E. V.; Griffin, R. G.; Dobson, C. M. Atomic structure and hierarchical assembly of a cross-β amyloid fibril. *Proc. Natl. Acad. Sci. U. S. A.* **2013**, *110* (14), 5468−5473.
(52) Boettcher, C.; Stark, H.; van Heel, M. Stacked bilayer helices: a new structural organization of amphiphilic molecules. *Ultramicroscopy* **1996**, *62* (1−2), 133−9.
(53) Lafleur, R. P. M.; Schoenmakers, S. M. C.; Madhikar, P.; Bochicchio, D.; Baumeier, B.; Palmans, A. R. A.; Pavan, G. M.; Meijer, E. W. Insights into the Kinetics of Supramolecular Comonomer Incorporation in Water. *Macromolecules* **2019**, *52* (8), 3049−3055.
(54) Fejer, S. N.; Wales, D. J. Helix Self-Assembly from Anisotropic Molecules. *Phys. Rev. Lett.* **2007**, *99* (8), 086106.

https://dx.doi.org/10.1021/jacs.0c08179
J. Am. Chem. Soc. 2020, 142, 17644−17652